American Mineralogist, Volume 84, pages 1883–1894, 1999

Metastable non-stoichiometric diopside and Mg-wollastonite: An occurrence in an interplanetary dust particle

FRANS J.M. RIETMEIJER

Institute of Meteoritics, University of New Mexico, Albuquerque, New Mexico 87131, U.S.A.

ABSTRACT

Interplanetary dust particles (IDPs) are the best samples available for the study of the dust that accreted in the early solar system to form protoplanets at 4.56 Ga. Chondritic aggregate IDPs have a matrix of (sub)-spherical units with variable amounts of micrometer-sized Fe,Ni-sulfides, Mg,Fe-olivines, and (Ca,Mg,Fe)-pyroxenes. The crystallographic and chemical properties of these materials can be modified by energetic thermal processes such as irradiation by energetic atoms (space weathering) and flash heating when an IDP decelerates in the Earth's upper atmosphere. Both thermal events have high heating and quench rates. Thermal alteration that occurs during atmospheric entry, or dynamic pyrometamorphic alteration, could obscure many details of earlier thermal modifications. Pure and TiO_2- or Al_2O_3-bearing, non-stoichiometric diopside and Mg-wollastonite in the IDP L2011K7 are the ultimate products of these thermal modifications, which were dominated by thermally induced loss of (Ca,Mg)O or mostly MgO in original Ca,Mg-clinopyroxene. The calculated oxygen deficiencies, O = 22 – 24 atoms per formula unit (afu) on the basis of Si = 8.00 afu, support a sequence of "anhydrous biopyriboles": diopside/Mg-wollastonite → anhydrous amphibole → (Si-rich) anhydrous smectite. This particular type of thermal modification, which is kinetically controlled, is unique to the constituents of IDPs. The extreme environmental conditions of high temperatures with high heating and cooling rates encountered by IDPs favor metastable equilibrium of the reaction products. That is, the kinetic, non-equilibrium processes, do not yield random reaction products but ones with predictable chemical compositions. The Ca,Mg-clinopyroxene compositions observed in this IDP were determined by the metastable eutectic in the enstatite-wollastonite system. The "anhydrous biopyribole" reaction sequence breaks down at calculated oxygen deficiency (O< 20 afu) in the vesicular, amorphous, amoeboid grains that could have been melted by atmospheric-entry flash heating.

INTRODUCTION

Several lines of evidence indicate deviations from ideal stoichiometry in pyroxene altered at very high temperatures. Non-stoichiometric Mg,Ca-clinopyroxene domains, which consist of two intergrown phases with 15 and 51 mol% $CaSiO_3$, formed during thermal decomposition of tremolite were reported by Xu et al. (1996). An experimental study of the system diopside-H_2 at $P_{H_2} = 10^{-6}$–10^{-9} bar between 1200–1500 °C showed systematic Ca/Mg increases in partially evaporated diopside at temperatures above the vaporous (Mysen et al. 1985; Table 1: 2412liq.; $En_{45.4}Wo_{54.6}$). Synthetic aluminous enstatite with "excess SiO_2," or Mg/Si <1, showed substitution by a hypothetical Mg-Eskola pyroxene, $Mg_{0.5}Al[Si_2O_6]$, with vacancies in the large (M_2) cation sites (Fockenberg and Schreyer 1997). The rapidly formed, non-equilibrium crystalline phases in these studies have the descriptive structural formula $(Mg,Ca)_{2-x}Si_{2+0.5x}O_6$. The thermally produced Ca,Mg-silicates in tremolite had randomly distributed (Ca,Mg)O vacancies and resembled "anhydrous" tremolite, $(Ca,Mg)_7Si_8O_{23}$ (Xu et al. 1996). Similar non-stoichiometric Ca,Mg-silicates in chondritic interplanetary dust are the subject of this paper.

Interplanetary dust particles (IDPs) are predominantly debris from impact erosion of (1) asteroids in a belt between Mars and Jupiter and icy-bodies in the Kuiper belt beyond Neptune's orbit, and (2) cometary dust released during perihelion passage when ice sublimation releases embedded dust from the nucleus. After liberation from a parent body, an IDP spends 10^4–10^5 years in interplanetary space and slowly spirals toward the sun under Poynting-Robertson drag. When it crosses the Earth's orbit, there is an opportunity for the IDP to be captured by the Earth's gravitational field (Brownlee 1985). Typical Earth encounter velocities range from 11 to >20 km/s. In the atmosphere between ~120–80 km altitude, an incoming IDP decelerates to velocities of cm/s in 5–15 s via collisions with air molecules. A large fraction of the kinetic energy contributes to flash heating whereby the interior of a typical IDP, ~10–20 μm in diameter, reaches a uniform temperature that varies as a function of particle size and mass, its entry velocity, and entry angle (Brownlee 1985). The physical parameters of this process are understood well enough to calculate the resulting time-temperature profiles in IDPs (Love and Brownlee

*E-mail: fransjmr@unm.edu

0003-004X/99/1112–1883$05.00

1991) during flash heating up to 1150 °C and rapid cooling at 10^5–10^6 °/h (Rietmeijer 1996a).

All IDPs experience some level of thermal alteration. This alteration in IDPs is known as "dynamic pyrometamorphism" (Rietmeijer 1998), but the term here does not imply the action of deformation processes as it does for terrestrial rocks. Dynamic pyrometamorphism is characterized by: (1) diffusionless oxidation and reduction reactions; (2) formation of cotectic and thermal minimum melts (Rietmeijer et al. 1999a); (3) volatile element loss (e.g., sulfur, zinc); and (4) nucleation of Mg,Fe-silicates and Fe-oxides (<50 nm in size) in amorphous ferromagnesiosilica materials (Rietmeijer 1996b, 1998). It is the final thermal alteration that an IDP experiences prior to being collected.

Sputtering by energetic H and He nuclei can modify anhydrous silicates in IDPs prior to accretion by forming a rim on enstatite (Bradley 1994) and forsterite (Rietmeijer 1996b) characterized by a bulk stoichiometric excess of O and depletion of Mg. The crystal structure in the rim was destroyed and its composition was changed relative to the underlying crystalline phase during exposure to the space environment (Bradley 1994). Energetic solar flare particles leave randomly oriented linear tracks along which the olivine and pyroxene lattice was destroyed (Bradley et al. 1988).

The primitive aggregate IDPs with an approximately chondritic bulk composition consist of a matrix of (sub)spherical units (~0.1–3 μm in diameter) that include: (1) amorphous units; (2) ultrafine-grained ferromagnesiosilica units; and (3) coarse-grained, holocrystalline ferromagnesiosilica units having variable Al and Ca (Bradley 1994; Rietmeijer 1989, 1998; Brownlee et al. 1999). Variable amounts of micrometer-sized Fe,Ni-sulfide, Mg,Fe-olivine, and (Ca,Mg,Fe)-pyroxene grains are embedded in the matrix. The pyroxenes include Ca-free ($En_{100–70}$) and low-Ca (0–15 mol% and ~25 mol% $CaSiO_3$) phases, diopside (~40–55 mol% Wo) and Ti-diopside (Germani et al. 1990; Zolensky and Barrett 1994). I report here the analytical-electron-microscope (AEM) data for non-stoichiometric diopside and Mg-wollastonite that were produced in a chondritic aggregate IDP by sputtering in space (space weathering) and dynamic pyrometamorphism. The resulting metastable-eutectic compositions of clinopyroxene are predicted by phase relations in the Enstatite (En)-Wollastonite (Wo) system.

Experimental procedures

Collection and curation

In 1976 it became possible to collect IDPs routinely in the stratosphere between 17–19 km altitude using inertial-impact, flat-plate collectors mounted underneath the wings of high-flying aircraft. The review articles by Mackinnon and Rietmeijer (1987), Bradley et al. (1988), and Rietmeijer (1998) presented the petrology of IDPs, their major- and minor-element and isotopic compositions, and noble gas abundances. Warren and Zolensky (1994) and Rietmeijer and Warren (1994) provided details on the collection and curation procedures of the NASA Johnson Space Center Cosmic Dust Program. The surface of collectors is covered with a layer of high-viscosity silicone oil to entrap impacted dust. Particles were handpicked off the collector and rinsed with hexane. This procedure is not fully efficient and a monolayer of silicone oil remains on rinsed particles. Its presence is not a problem during major-element analysis (using an energy-dispersive spectrometer) of grains located in IDP interiors in serial ultra-thin sections (Rietmeijer 1987, 1998). Individual particles receive a preliminary identification that is published in the NASA Cosmic Dust Catalogs (Mackinnon et al. 1982; Warren and Zolensky 1994).

TEM/AEM analyses

Particle L2011K7 was embedded in epoxy (Spurrs). Serial sections were prepared using a Reichert-Jung Ultramicrotome E. The ultra-thin (90 nm) sections were placed on holey carbon thin-films that were supported by standard 200 mesh Cu grids for study in a JEOL 2000FX AEM. The AEM operated at an accelerating voltage of 200 keV and was equipped with a Tracor-Northern TN-5500 energy-dispersive spectrometer (EDS) for analysis of elements with atomic number >11. The analytical spot size was ~15 nm in diameter. Quantitative data were obtained using the Cliff and Lorimer (1975) thin-film correction procedure and experimentally determined *k*-factors on natural standards (Mackinnon and Kaser 1987). The error in abundances of major-element oxides is 5% relative. Of course, the accuracy and precision of EDS analysis cannot compete with wavelength dispersive, electron-microprobe analysis but the size of these silicates in ultrathin sections precluded use of the latter technique. Care was taken to ensure that the EDS probe

Table 1. Representative analyses showing chemical variations within two diopside single crystals (1-4 and 5-7) in aggregate IDP L2011K7

Grain size (nm)	758				1005		
Texture	smooth				smooth		vesicular
Analyses	1	2	3	4	5	6	7
SiO_2	65.7	64.7	62.8	63.1	65.2	58.7	84.9
Al_2O_3		3.3	3.9	2.4		2.7	
MgO	16.6	15.7	14.2	16.6	16.3	16.1	7.4
CaO	17.7	16.3	18.5	17.9	18.5	21.3	7.7
TiO_2			0.5			1.2	
Structural formulae normalized to Si = 8.00							
Al		0.48	0.59	0.36		0.43	
Mg	3.01	2.89	2.70	3.14	2.98	3.27	1.04
Ca	2.31	2.16	2.53	2.43	2.43	3.11	0.78
Ti			0.05			0.12	
$O_{(calculated)}$	21.32	21.77	22.22	22.11	21.41	23.27	17.82
En	56.6	57.4	51.8	56.3	55.2	51.2	57.4
Wo	43.4	42.6	48.2	43.7	44.8	48.8	42.6

only included a grain that was free of matrix material and visible inclusions. The probe size and beam current were monitored during EDS analyses to ensure reproducible conditions. For determination of its thickness, a grain was imaged with the sample at two different tilt angles relative to the incident electron beam. The resulting data are free of experimental artifacts. To test the accuracy and precision of the EDS analyses, a powdered sample of a pure diopside standard was prepared in the same manner for AEM analyses as was the IDP. The ultrathin sections of the standard were analyzed under similar experimental conditions and reduced using the same thin-film correction procedure. The relative error in interplanar (*d*-) spacings for single crystals of clinopyroxene in the IDP obtained from selected-area electron diffraction (SAED) patterns is 2%.

OBSERVATIONS

The Ca,Mg-silicate in IDP L2011K7, which is 22×17 μm in cross section, is embedded in a matrix of ferromagnesiosilica units that preserve the original accretion texture (Fig. 1). There is a sharp interface between the grains and spherical matrix units that are vesicular at the interface (Fig. 2). There is no evidence for chemical zoning in Ca,Mg-grains toward this interface. Rare grains show local, concentric circular, strain contrast. A few single-crystal grains contain solar-flare tracks (Fig. 3). The grains occur as euhedral to subhedral single crystals, amoeboid grains with convex boundaries impinged at discrete locations on the grain boundary, and as rare grains with a smooth surface and rounded edges (Figs. 4a). A few rounded, subhedral grains contain scattered, randomly oriented, Fe-oxide nanocrystals in a featureless matrix (Fig. 4b). These nanocrystals range from 1–9 nm in size (mean = 3.3 nm; 1σ = 2.0 nm; mode = 2.7 nm). Many grains contain circular vesicles (Fig. 5a) that are commonly concentrated in discrete domains. The largest vesicles (~20 nm) have a negative crystal shape. In grains with large vesicles, the iron oxide nanocrystals (Fig. 5b) locally form linear arrays whereby areas of high nanocrystal density contain up to 0.5 wt% FeO. One grain has a spotty distribution of circular patches (15–50 nm in diameter) consisting of ~90 wt% SiO_2 and ~10 wt% CaO + MgO. Two perpendicular dimensions, $a > b$, were measured across each grain. The root-mean-square size

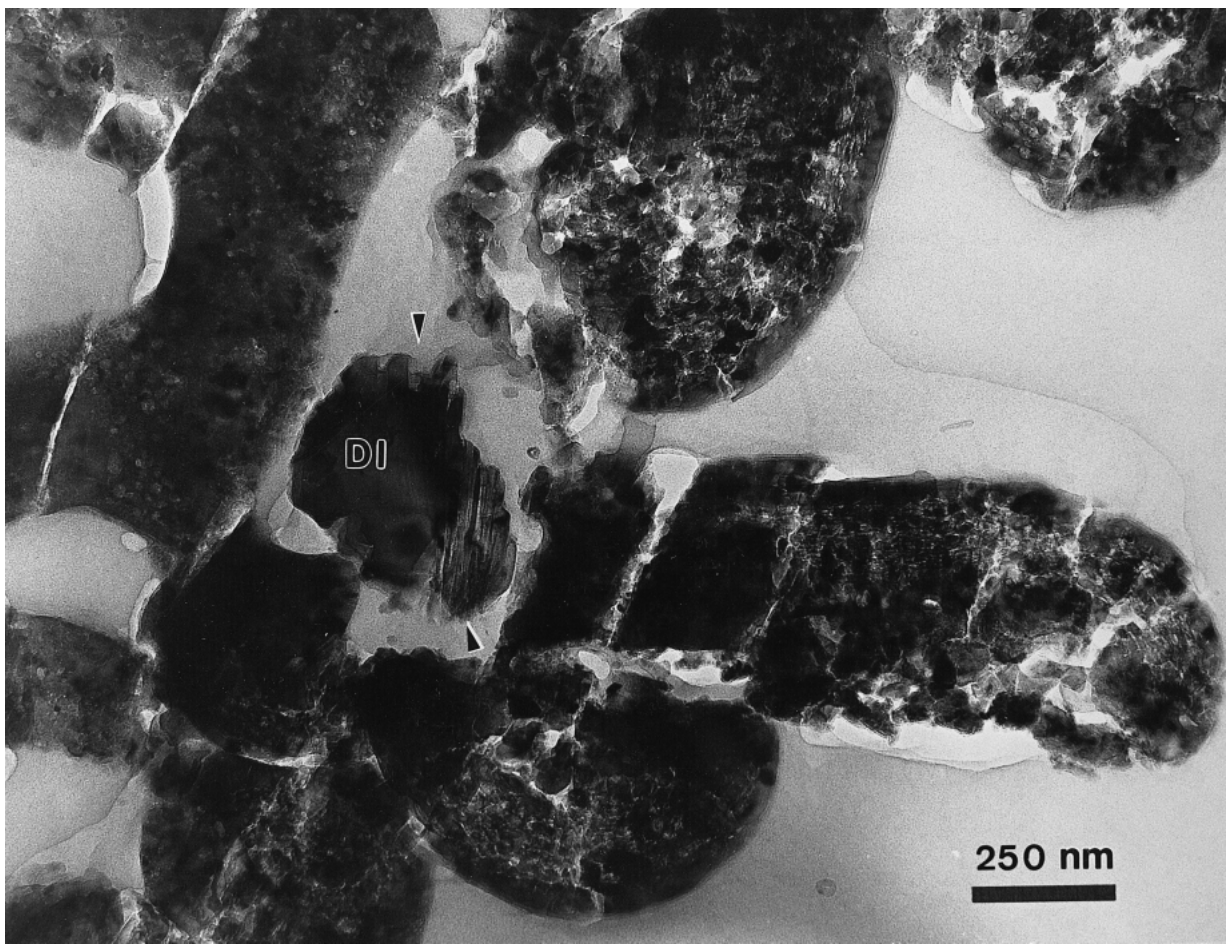

FIGURE 1. TEM micrograph of the dust-accretion texture in aggregate IDP L2011K7 with diopside (DI) single crystals showing thermal stress lamellae (arrows) surrounded by ultrafine-grained ferromagnesiosilica matrix units. Elongated shapes result from fusion of originally (sub-) spherical units.

FIGURE 2. TEM micrograph of aggregate IDP L2011K7 showing the interface between a single crystal of diopside (DI) and a ferromagnesiosilica matrix unit with a large vesicle at the interface (white arrow). Lineation in the unit probably indicates heating close to its melting point followed by rapid quenching.

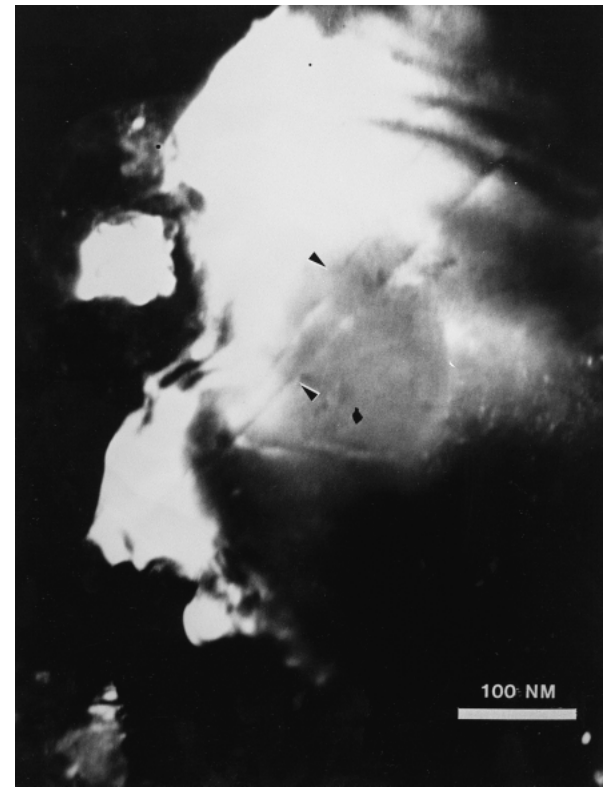

FIGURE 3. Dark-field TEM micrograph showing solar flare-tracks in diopside in IDP L2011K7.

TABLE 2. Representative analyses of subhedral diopside and Mg-wollastonite single crystals (1-6) and irregular amorphous grains (7) in aggregate IDP L2011K7

Grain size (nm)	545		617		174	732	315	801
Texture	smooth	lamellae	lamellae		smooth			
Analyses	1	2	3	4	5	6	7	8
SiO_2	60.7	76.3	75.6	60.2	62.5	59.1	83.5	54.5
Al_2O_3				5.2				
MgO	17.3	12.2	10.9	10.9	15.1	16.4	6.0	16.9
CaO	22.0	11.5	13.4	19.2	22.4	23.1	10.5	27.1
TiO_2				4.4		1.4		1.3
Structural formulae normalized to Si = 8.00								
Al				0.81				
Mg	3.40	1.91	1.72	2.16	2.88	3.31	0.87	3.70
Ca	3.11	1.29	1.52	2.73	3.07	3.35	1.08	4.26
Ti				0.44		0.14		0.14
$O_{(calculated)}$	22.51	19.20	19.24	22.99	21.95	22.94	17.95	24.24
En	52.3	59.5	53.5	44.1	48.5	49.7	44.5	46.5
Wo	47.7	40.5	46.5	55.9	51.5	50.3	55.5	53.5

Note: Two grains (1-2) and (3-4) have (110) fracture lamellae; diopside crystal (6) contains solar flare tracks.

[rms = $(a^2 + b^2)^{1/2}$] displays a skewed (S = –0.9) normal distribution with mean = 587 nm (1σ = 207.9 nm; range = 141–1005 nm). The smallest grains have a circular cross section.

The euhedral and subhedral grains typically have a well-defined, single-crystal SAED pattern (Fig. 6). The SAED patterns for most of the amoeboid grains lack diffraction maxima indicating that they are amorphous. Several grains are partially fractured with sub-parallel (110) lamellae that are 10 nm to 59 nm wide (mean = 20.9 nm; 1σ = 12.4 nm; mode = 12.3 nm; S = 0.7). The SAED pattern in an orientation perpendicular to *hkl* 110 show that they are (slightly) rotated single-crystal lamellae (Fig. 6). The SAED data confirm the *C*2/c clinopyroxene space group with β = 106° (diopside), and a few single-crystals >50 mol% Wo that are Mg-wollastonite with β = 95° (Shinno 1974).

Representative EDS analyses across each of two large, texturally homogeneous, single crystals are reproducible (Table 1). Compositional varable 1, anal. 7; Table 3, anal. 1), thermal stress lamellae (Table 1, anal. 4; Table 2, anal. 2–4), and incipient

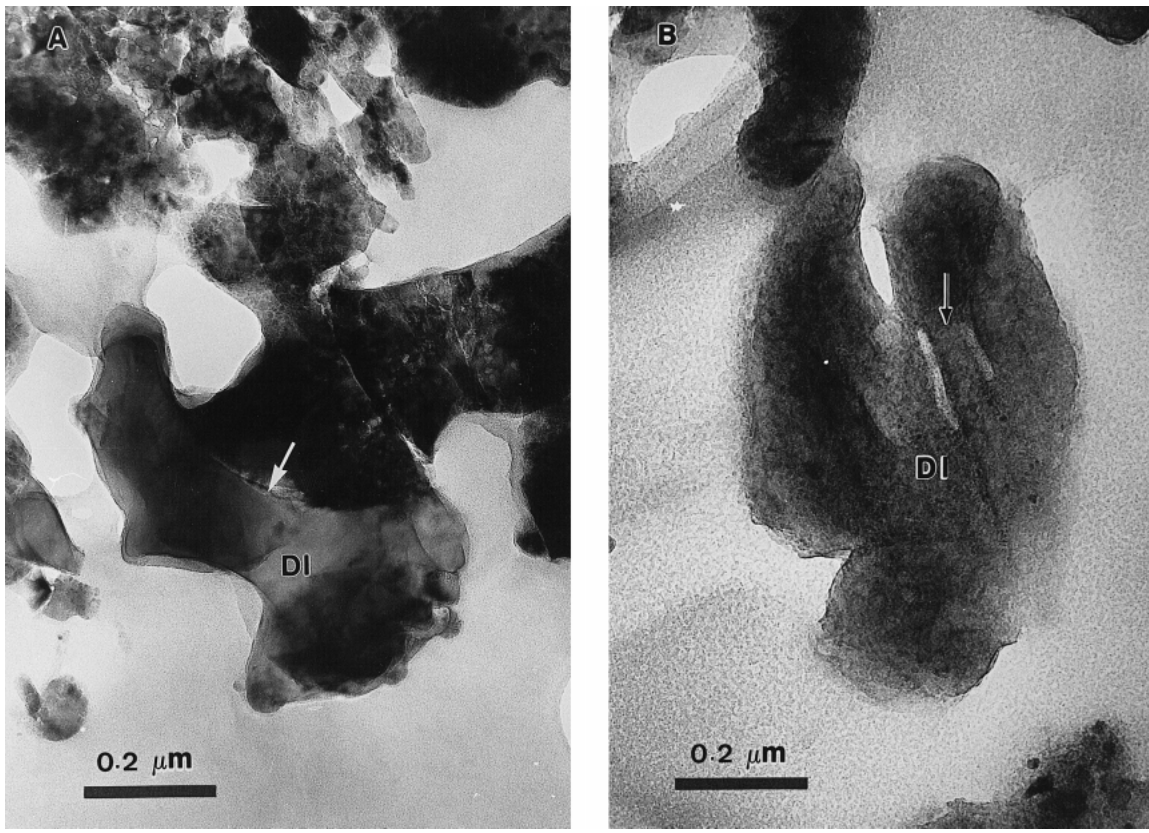

FIGURE 4. TEM micrographs of aggregate IDP L2011K7: (**A**) the sharp interface between and amoeboid diopside (DI) single crystal and a matrix unit, and (**B**) an irregularly shaped diopside (DI) grain with elongated vesicles (arrow) and scattered nanometer-sized iron oxides (black spots).

melt textures (Tables 1, anal. 7; Table 3, anal. 5 and 6). About 90% of grains contain Al_2O_3 and/or TiO_2 with the highest concentrations of these oxides generally in an ill-defined domain within a grain (Table 3, anal. 6 and 7). The wollastonite contents range from 37.1 to 61.8 mol% (mean = 50.5%; 1σ = 4.7; N = 68) and could mark a transition from clinopyroxene proper (≤50 mol% $CaSiO_3$) to a pyroxenoid (>50 mol% $CaSiO_3$; Shinno 1974). The single crystals include pure quadrilateral diopside, Al_2O_3-bearing diopside, and pure and Ti(±Al)–Mg-wollastonite (Table 4). The Ti(±Al)–bearing Mg-wollastonite grains and domains show a coupled substitution $CaTiAl_2O_6$ (Fig. 7). The observations suggest two possible models, as follows.

Model 1

Stoichiometric Ca,Mg-clinopyroxene is present but the majority is non-stoichiometric. Calculated on the basis of O = 6 afu, i.e., $(Mg,Ca)_{2-x}Si_{2+0.5x}O_6$, there is stoichiometric "excess Si", or 0.5x, in the formula (Table 4). High excess Si values are found in the irregularly shaped and rounded grains with the highest values for amoeboid grains with >55 mol% Wo. The sums of cations (Σ) range from 3.34 to 3.99 with Σ_{mean} = 3.79 (1σ = 0.13; mode = 3.88; N = 68) (Fig. 8). Only high-alumina (± TiO_2) clinopyroxene has Si <2.00 and ample Al to fill the tetrahedral site. A systematic deficiency in the remainder of the structural formula could indicate vacancies in the structure

TABLE 3. Representative analyses of Al- and/or Ti-bearing diopside and Mg-wollastonite single crystals in aggregate IDP L2011K7

Grain size (nm)	902	247	316	463	789	
Texture	vesicles	smooth	smooth	smooth	smooth	
Analyses	1	2	3	4	5	6
SiO_2	57.2	50.6	56.4	54.4	64.4	51.6
Al_2O_3		9.4	6.8	2.6		7.4
MgO	16.4	13.7	11.2	15.1	16.3	13.6
CaO	25.0	22.0	20.3	24.7	19.3	22.3
TiO_2	1.4	4.3	5.2	3.2		5.1
Structural formulae based on O = 6						
Si	2.06	1.80	1.98	1.95	2.22	1.84
Al_T		0.20	0.02	0.05		0.16
Al		0.20	0.26	0.06		0.15
Mg	0.88	0.73	0.59	0.81	0.84	0.72
Ca	0.96	0.84	0.76	0.95	0.71	0.85
Ti	0.04	0.12	0.14	0.09		0.14
Vacancy	0.12	0.11	0.25	0.09	0.45	0.14
excess Si	0.06				0.22	
Structural formulae normalized to Si = 8.00						
Al		1.75	1.14	0.45		1.35
Mg	3.42	3.23	2.37	3.31	3.02	3.14
Ca	3.75	3.73	3.09	3.89	2.57	3.70
Ti	0.15	0.51	0.55	0.35		0.59
$O_{(calculated)}$	23.47	26.61	24.27	23.88	21.59	26.05
En	47.8	46.4	43.8	46.0	54.0	45.9
Wo	52.2	53.6	56.2	54.0	46.0	54.1

Note: Grain 5 has a large Al,Ti-domain (6).

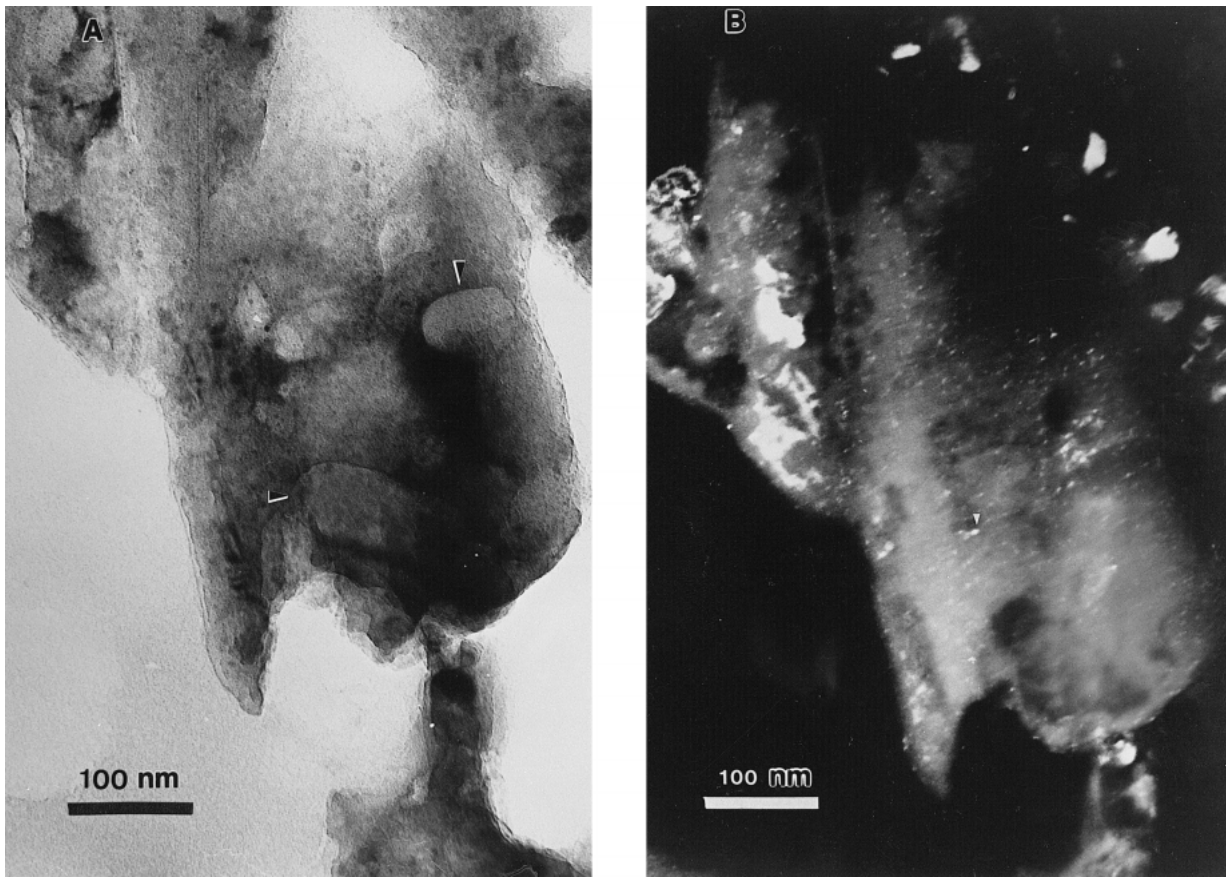

FIGURE 5. TEM micrographs of Ca,Mg-rich grains in IDP L2011K7: (**A**) bright-field image showing vesicles (arrows) and nanometer-sized iron oxides (black spots); (**B**) dark-field image of the same area showing the iron oxides (white spots).

(Table 3). Grains with excess-Si (Table 3; anal. 1) also could have had vacancies, although Al and Ti redistribution into domains could be involved (Table 3; anal. 6).

Model 2

Following the (Ca,Mg)O-vacancy model (Xu et al. 1996), vacancies could be formed in the thermally modified Ca,Mg-clinopyroxene in IDP L2011K7. When normalized to Si = 8.00, this model maintains the integrity of the pyroxene chain structure showing the stoichiometric (Ca + Mg) deficiency and O excess (Tables 1–3). The lowest calculated oxygen contents, O <20 (afu), occur in the Al- and Ti-free, vesicular, amorphous, amoeboid grains. The scatter of calculated O as a function of Mg (afu) (Fig. 9a) decreases significantly as a function of (Mg+Ca) (afu) (Fig. 9b). The oxygen vs. (Mg+Ca+Al+Ti) (afu) diagram shows a linear correlation that is offset from the ideal correlation due to the high (Al,Ti)-silicates with excess O (Fig. 9c). The data points below the correlation line are Al,Ti-bearing silicates. Excess calculated O correlates with high (Al ± Ti) in Mg-wollastonite. The calculated O content in the pure diopside standard ranges from 22.7–24.48 (Fig. 10). The mean value of calculated O is 23.5 (one standard deviation = 0.38). This result on the diopside standard shows that oxygen values below 23.5 indicate non-stoichiometric, i.e., O-deficient, clinopyroxene. To facilitate comparison of the models, the relationship of excess Si (based on O = 6) as a function of calculated O (based on Si = 8.00) is shown in Figure 11. The largest O deficits and maximum non-stoichiometry (or excess Si) occur in (Al,Ti)-free amorphous grains. The non-stoichiometry of diopside and Mg-wollastonite is a property that can be used to characterize their thermal history in this IDP.

DISCUSSION

Interplanetary dust particles are the best available samples to study the dust that accreted to form the early solar system protoplanets. Conditions in their icy parent bodies were not conducive to alteration that could greatly modify the original mineralogical properties of aggregate IDPs. They still contain a record of a complex history that spans the time from pre-IDP accretion processes to alteration that occurred shortly before IDPs were collected in the lower stratosphere. The highly energetic thermal processes that could efficiently induce mineral alteration in IDPs are sputtering and radiation by energetic atoms in space and flash heating during deceleration in the Earth's atmosphere. Both processes are characterized by high tempera-

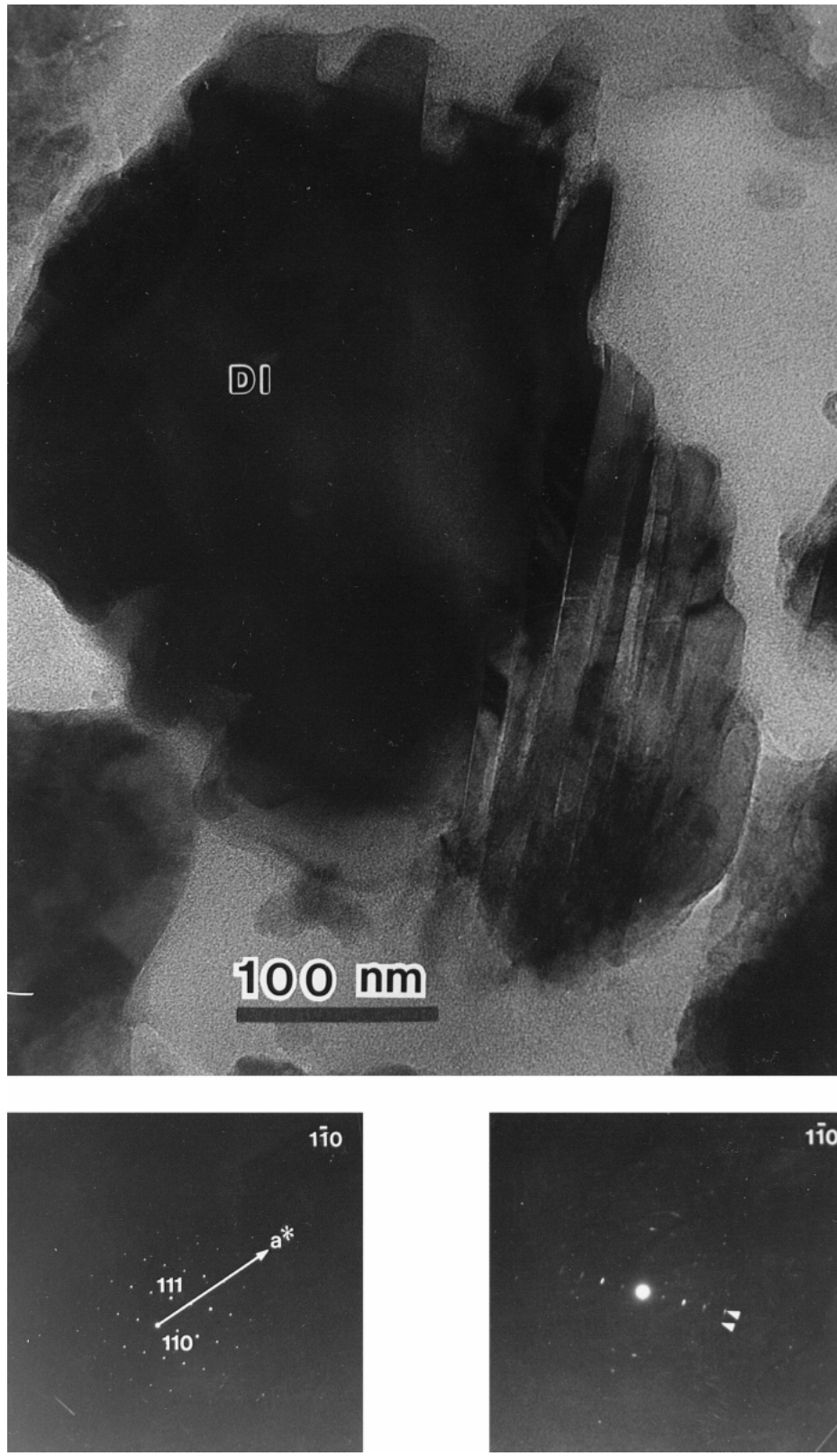

FIGURE 6. TEM micrograph of diopside in Figure 1 and a single-crystal SAED pattern (**bottom-left**) from the left-hand side of the grain and a SAED pattern (**bottom-right**) of slightly rotated (arrows) thermal stress lamellae.

TABLE 4. Chemical and formula characteristics of diopside (≤50 mol% Wo), Mg-wollastonite, and glass (>50 mol% Wo) in aggregate IDP L2011K7

		Diopside		Mg-Wollastonite and glass		
		Quadrilateral.Cpx	Al_2O_3-bearing Cpx	Quadrilateral.Cpx	TiO_2-bearing grains	Al_2O_3/TiO_2-bearing grains
Number of data		11	13	7	19	18
mol% Wo	mean	45.8	46.1	54.0	53.1	52.5
	σ	2.8	3.8	3.8	3.15	3.4
	range	43.4–50.0	37.1–50.0	51.0–61.8	50.1–58.7	47.4–60.4
excess Si	mean	2.31	2.33	2.20 [N= 5] [2.675; N= 2]	2.10	2.02
	σ	0.14	0.12	0.06	0.11	0.12
	range	2.12–2.50	2.02–2.45	2.16-2.30	1.98–2.44	1.80–2.28
Σ	mean	3.69	3.73	3.80 [N= 5] [3.33; N= 2]	3.86	3.82
	σ	0.13	0.11	0.05	0.11	0.09
	range	3.50–3.87	3.52–3.96	3.70–3.84	3.52–3.985	3.61–3.93
Al_2O_3 wt%	mean		1.93			4.1
	σ		1.35			2.0
	range		0.6–4.8			1.6-9.4
TiO_2 wt%	mean				1.34	2.6
	σ				0.60	1.5
	range				0.1–2.3	0.5–5.2

Note: Gaussian distributions are confirmed at a 95% confidence limit. Two amorphous amoeboid Mg-wollastonite grains that are not listed have excess Si = 2.7.

tures and by rapid heating and cooling rates. Bradley (1994) showed that irradiation by energetic nuclei produced Mg-depleted silicates with a bulk stoichiometric O excess. These amorphous grains and/or solar flare tracks in IDP silicates are unambiguous evidence that the grains, and by association the host IDP, traveled in space (Bradley et al. 1988).

When meteorites enter the Earth's atmosphere, they develop a fusion crust of a few millimeters of thickness underneath which the rock remains thermally unaffected (Ramdohr 1967). This situation is different for decelerating IDPs that generally establish thermal equilibrium between the surface and interior (Love and Brownlee 1991). Phase transformations in constituent phases could cause a thermal gradient. Formation of the thermal gradient depends critically on the IDP size, although the exact nature of this relationship remains untested (Flynn 1995). This flash-heating event that induces dynamic pyrometamorphic alteration occurs between 100–80 km altitude, where $P_{H_2} \sim 10^{-12}$ bar and $P_{O_2} \sim 10^{-8}$ bar (U.S. Standard Atmosphere 1976). Thermal modifications that indicate an extraterrestrial origin (Fraundorf 1981; Rietmeijer 1998) of IDP L2011K7 include: (1) a (partial) iron-oxide rim (<100 nm thick); (2) decorations of Fe-oxide nanocrystals in rare Ca,Mg-grains with traces of iron; (3) vesicles (degassing); (4) (110) fracture lamellae; and (5) fused matrix units. Fraundorf et al. (1982) showed that solar-flare tracks in olivine were erased by flash heating above ~600 °C. The response of similar tracks in Ca,Mg-clinopyroxene is unknown. In IDP L2011K7, solar-flare tracks occur in some grains but not in others. The failure of tracks to anneal in some grains might indicate that a thermal gradient kept the internal IDP temperature below the track flash-heating annealing temperature, whereas other grains were already weakened structurally due to vacancies that existed prior to atmospheric entry, which facilitated track erasure at lower temperatures.

Metastable, non-stoichiometric diopside, and Mg-wollastonite

It is conceivable that structurally weakened, non-stoichiometric, Ca,Mg-clinopyroxene in IDP L2011K7 formed before incorporation into this IDP and that pre-accretionary radiation created the (Ca,Mg)O vacancies. The observed correlation between deviations from the ideal structural formula and grain morphology would lend support to the notion that precursors to the amorphous grains contained more vacancies than did single-crystal grains with solar-flare tracks. The former became amorphous at temperatures below the (unknown) flash-heating annealing temperature of solar-flare tracks in diopside. The single-crystal grains suffered variable levels of modification during this final thermal event, such as local Al_2O_3 and/or TiO_2 enrichments. It is uncertain whether Si-rich patches (Table 1, anal. 7) are a primary feature or a readjustment of the amount of Si in solid solution to the conditions of pyroxene and pyroxenoid stability after peak heating.

The very nature of both thermal events promotes metastable equilibrium during kinetically controlled thermal alteration. The formation of solids with metastable eutectic compositions was observed in aluminosilica solids condensed from the vapor phase (Rietmeijer and Karner 1999) and in the nanometer-sized reaction products in a triggered-lightning experiment (Rietmeijer et al. 1999a). A study of diopside (~175 μm in diameter) evaporation at $P_{H_2} = 10^{-6}$–10^{-9} bar between 1200–1500 °C (Mysen et al. 1985) may help to explain the IDP data. That study showed systematically increased Ca/Mg at temperatures above the vaporous suggesting preferential loss of Mg compared with Ca. The scatter of data points (Fig. 9a) could support the interpretation that mostly MgO vacancies were involved in the IDP.

The question becomes what is the driving force for the meta-

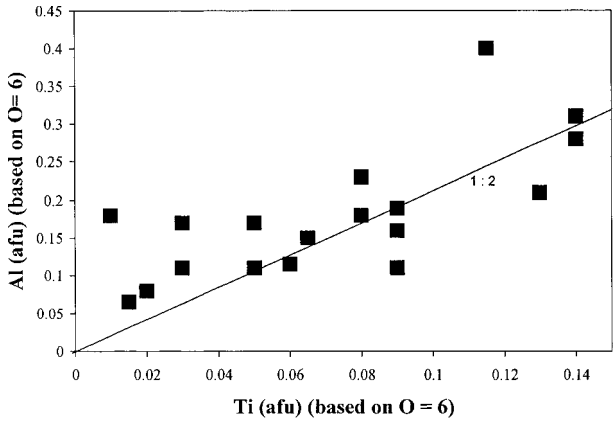

FIGURE 7. Ti vs. Al (atoms per formula unit, afu, on the basis of O = 6) in Mg-wollastonite in IDP L2011K7. The line labeled 1:2 corresponds to coupled substitution $CaTiAl_2O_6$.

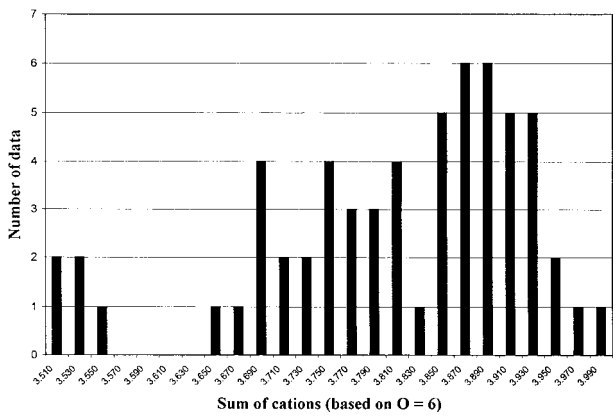

FIGURE 8. Histogram of the observed sum of cations (Σ) based on O = 6 in Mg,Ca-grains in IDP L2011K7. One value, Σ = 3.34, is omitted from this graphical presentation.

stable formation of non-stoichiometric diopside and Mg-wollastonite. Neither the En-Di (Huebner 1980) nor Di-Wo (Shinno 1974) phase diagrams have a metastable eutectic, but the composite diagram shows a metastable eutectic matching the observed Wo contents of the IDPs (Fig. 12). Diopside non-stoichiometry must have a limit beyond which its structure transforms to a pyroxenoid. With increased Ca/Mg, diopside gradually changed to metastable Mg-wollastonite that nucleated in a glass phase within the Wo_{ss} + Di stability field at ~900 °C (Shinno 1974) (Fig. 12). The observed non-stoichiometric diopside and Mg-wollastonite compositions are a predictable phenomenon in rapidly heated and quenched Ca,Mg-clinopyroxene.

In Figure 11, note that a modal value of 0.25 for excess Si (x) corresponds to a range of calculated O deficiencies from O = 22 – 24 (afu). The introduction of random (Ca,Mg)O vacancies in $(Ca,Mg)_8Si_8O_{24}$ yields $(Ca,Mg)_7Si_8O_{23}$, an "anhydrous amphibole" composition. The range of oxygen deficiencies spans an "anhydrous biopyribole" sequence starting with stoichiometric diopside and Mg-wollastonite to anhydrous amphibole to

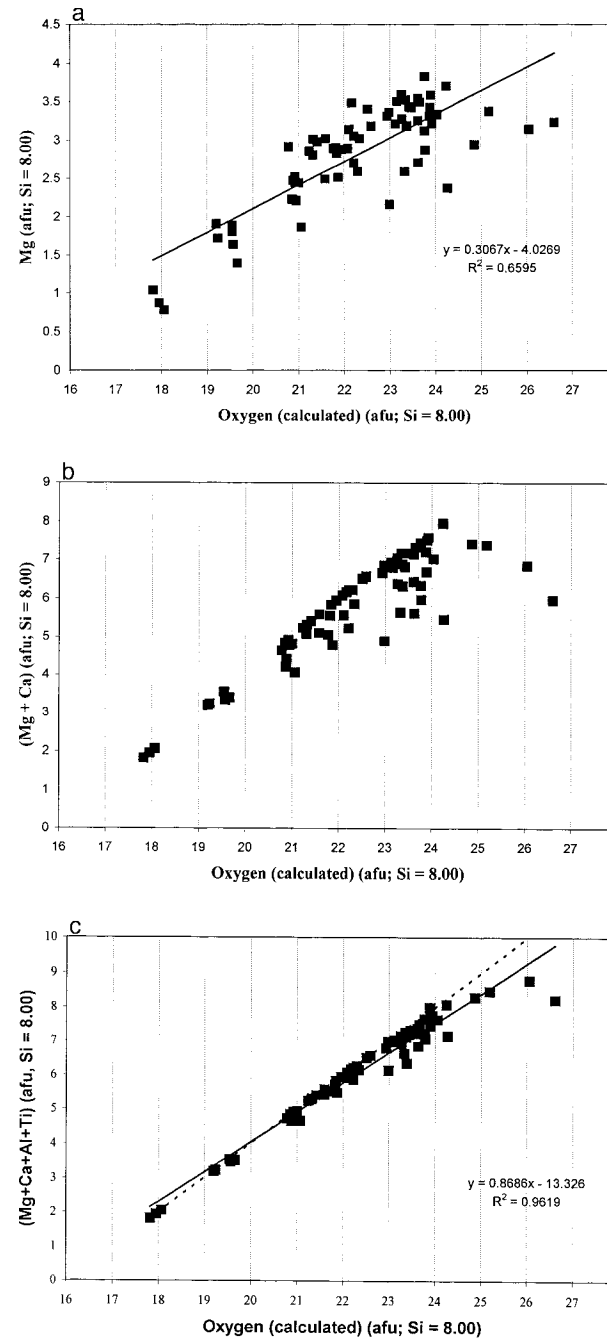

FIGURE 9. Calculated oxygen (afu) in non-stoichiometric diopside, Mg-wollastonite, and Al- and Ti-free amorphous grains in IDP L2011K7 on the basis of Si = 8.00 as a function of (**a**) Mg afu, (**b**) (Mg+Ca) afu, and (**c**) (Mg+Ca+Al+Ti) afu. The solid line in **a** and **c** is linear correlation through the data shown in **a**. The dashed line in **c** is the linear correlation through the data for the aluminous enstatite compositions with a hypothetical substitution $Mg_{0.5}Al[Si_2O_6]$ (Fockenberg and Schreyer 1997).

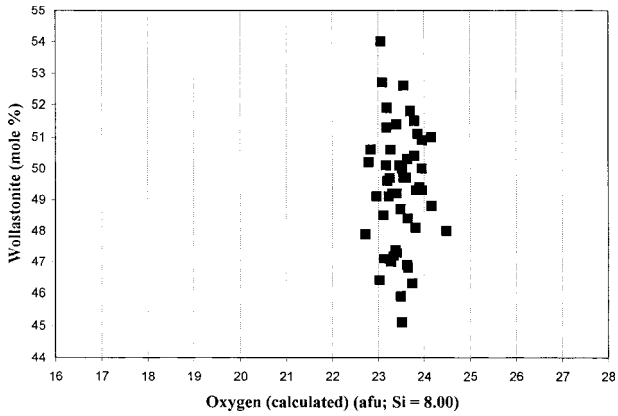

FIGURE 10. Calculated oxygen (afu) on the basis of Si = 8.00 in the diopside standard as a function of its Wo content, which ranges from 45.1 to 54.0 mol% with an average of 49.3 mol% (one standard deviation = 1.9)

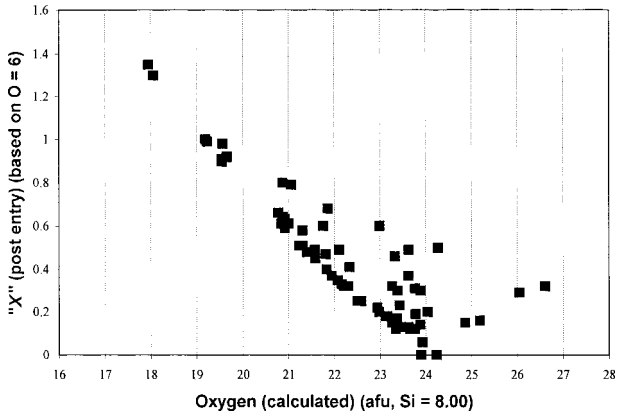

FIGURE 11. The correlation between calculated O (based on Si = 8.00) and excess Si (or "*x*") on the basis of O = 6 in non-stoichiometric diopside, Mg-wollastonite, and in Al- and Ti-free amorphous grains in IDP L2011K7

(Si-rich) anhydrous smectite with calculated O = 22, and beyond $Mg_5Si_8O_{21}$ (Fig. 9c). This sequence of variable M^{2+}/O for Si = 8.00 (afu) is interpreted as a kinetic response to thermal alteration. Vapor-condensed amorphous "MgSiO" and "FeSiO" solids showed well-defined compositions that match the metastable eutectics in the MgO-SiO_2 (Nuth et al. 1999) and FeO/Fe_2O_3-SiO_2 (Rietmeijer et al. 1999b) phase diagrams. In an MgO-(FeO/Fe_2O_3)-SiO_2 diagram, these eutectics predict that a Si-rich smectite dehydroxylate is the only possible metastable phase (Rietmeijer 1999). Thus, I submit that a kinetic response of thermally altered pyroxenes in IDPs will reach metastable equilibrium at $(Ca,Mg)_6Si_8O_{22}$–like compositions.

Assuming that the chemical response predominantly involved Mg-loss, then the formula, $(Mg,Ca)_{2-x}Si_{2+0.5x}O_6$, can be used to recalculate the original stoichiometric Ca,Mg-clinopyroxene compositions. The amount of MgO loss is $[(1.5x)/6] \times 40.32A$, where A is the sum of the atomic proportions of O for each molecule calculated from the original analysis and x represents excess Si (see Table 4). The original wollastonite contents ranged from 14 to 55 mol%, with mean Wo = 29.2 mol% in Ti-free cpx and 42.0 mol% in Ti-bearing clinopyroxene. The (110) fracture lamellae were probably intergrowths of Ca-poor (~18 mol% Wo) and Ca-rich (~35 mol% Wo) pyroxenes. The thermal stress lamellae could have formed during quenching following flash heating of clinopyroxene in the IDP because of different thermal expansion and contraction coefficients. The original Ti-bearing (Al-free) clinopyroxene had Σ(mean) = 3.98 (1σ = 0.015; range 3.94–4.00; N = 19), which was probably present as $\square_{0.5}CaTi_{0.5}Si_2O_6$ with 3.5 cations per unit formula. In this case, the average abundance (7 mol%) of this molecule yields Σ = 3.97 (based on O = 6). This Ti-bearing clinopyroxene probably already contained substitutional vacancies prior to thermal modification.

Iron-free clinopyroxene in IDPs could have formed during solar nebula condensation or thermal annealing of amorphous materials. Equilibrium condensation models predict pure diopside formation in a cooling solar-nebula gas at 1125 °C (Grossman and Larimer 1974), but evidence for equilibrium condensation based on studies of meteorites is still lacking. Vapor-phase condensates are typically fluffy particles of nanometer-sized grains (Stephens and Kothari 1978) that would require post-condensation processing to transform these particles to single crystals. This condensation scenario cannot be eliminated based on our current understanding of the physical processes during solar-system formation, which included igneous activity and metamorphism in asteroids (Kerridge and Matthews 1988). Aggregate IDPs commonly contain amorphous aluminosilica materials with variable CaO, MgO, and FeO contents (Rietmeijer 1998). It is possible that Ca,Mg-clinopyroxene formed originally in these materials, but at present there are no observations to support this notion.

The data for non-stoichiometric diopside and Mg-wollastonite in the IDP L2011K7 reveal a complex thermal history of sputtering and dynamic pyrometamorphism. The temperatures of these thermal events cannot be reconstructed because thermal modification was facilitated by structural vacancies and possibly affected by the surface free energy of these small (<1 μm) Ca,Mg-silicate grains. The dominant role of (Ca,Mg)O (or mostly MgO) vacancy formation in originally pure, and TiO_2 and/or Al_2O_3-bearing, pigeonite and diopside caused chemical changes that proceeded as an anhydrous biopyribole sequence. The final diopside and Mg-wollastonite represent kinetically controlled thermal modifications described by the composition of the metastable eutectic in the En-Wo phase diagram. This alteration in IDPs is not a chaotic non-equilibrium phenomenon but is entirely predictable.

The observations presented here show unusual features in a mineral group (clinopyroxene) that is typically compositionally well-behaved and a faithful recorder of its history. Of course, the vast body of knowledge about pyroxenes comes from studies of terrestrial crystalline rocks and only recently has it been shown that pyroxenes may develop some unusual

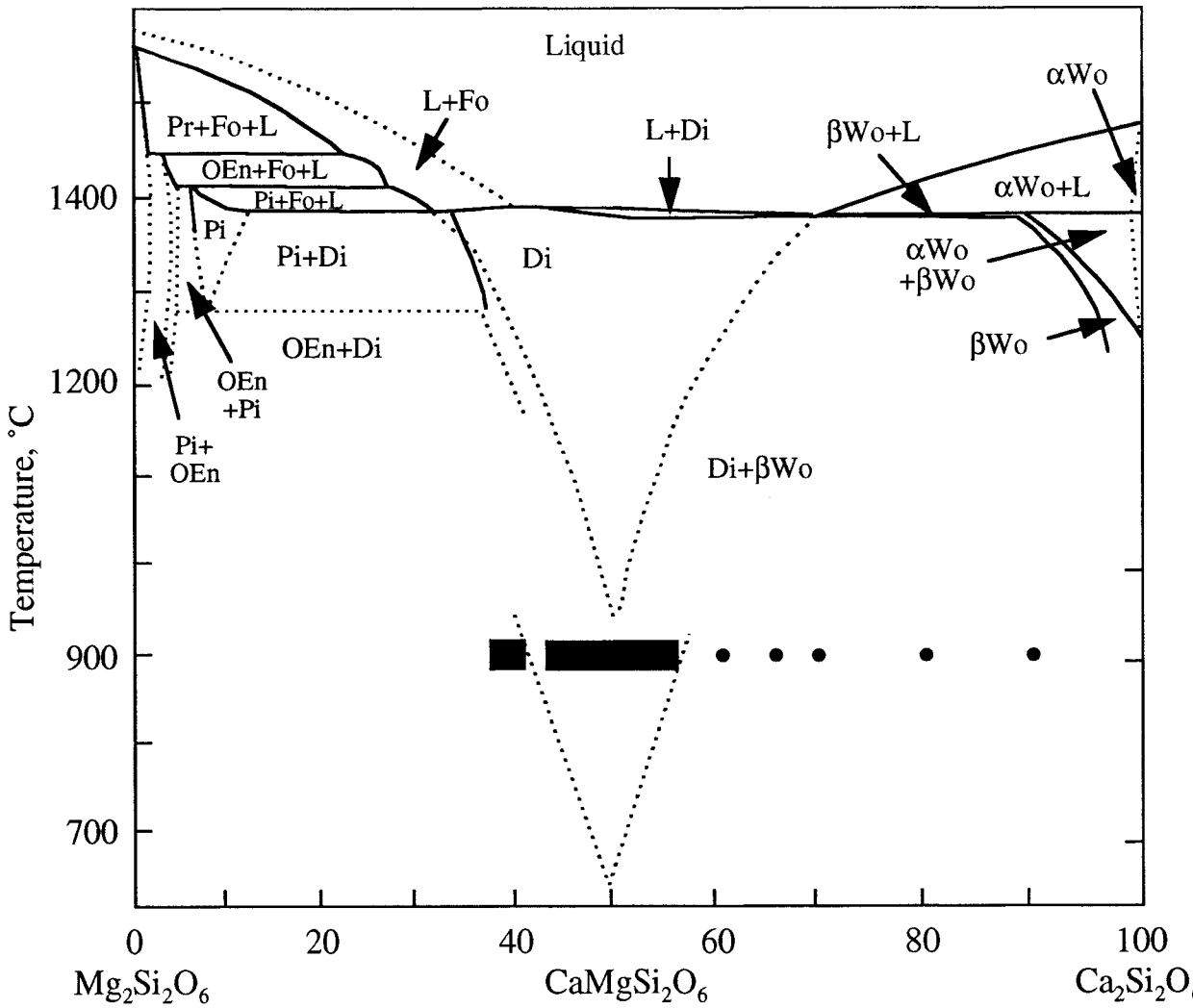

FIGURE 12. Computer-generated composite of the enstatite-diopside (Huebner 1980) and diopside-wollastonite (Shinno 1974) diagrams. There is an uncertainty in the match between the original diagrams. Thus, the phase field Di + Fo + L in the original Enstatite-Diopside diagram is not indicated in this composite diagram. The dashed lines merging toward the diopside composition denote the metastable eutectic in the composite diagram and its offset that straddles the compositions in IDP L2011K7 (black bars) compared to metastable β (Mg-) wollastonite (Shinno 1974; black dots).

features under mantle conditions and in deep-seated anorthosite massifs (Dymek and Gromet 1984). The pyroxene properties reported in this paper are the result of a history in extreme environments: (1) unknown modification of vapor-condensed solids to form the original mineral; (2) space weathering by high-energy atoms colliding with the original pyroxenes; and (3) dynamic pyrometamorphism in the upper atmosphere that is characterized by high temperatures and high heating and quenching rates. This kind of evolution ultimately may produce highly unusual if not unique features. The thermal events recorded in these clinopyroxene minerals can be separated in time by at least 4.56 billion years. Much detail of earlier sputtering-induced thermal modifications can become obscured during dynamic pyrometamorphism that occurred during atmospheric-entry flash heating. In this regard, the recently launched NASA STARDUST Discovery mission could provide critical information. This mission will collect dust at comet P/Wild 2 during its 2003/2004 perihelion for laboratory analyses. Because atmospheric-entry flash heating will not modify this collected dust, it is an excellent probe to study the nature the origin of non-stoichiometry in silicates that might date from the time of solar-system accretion.

ACKNOWLEDGMENTS

This paper benefited from critical reviews by M. Zolensky, R.F. Dymek, G.J. Flynn, and the Associate Editor, B.J. Jolliff. I acknowledge helpful discussions with Jim Papike, Case Klein, and Huifang Xu. The work was performed at the Electron Microbeam Analysis Facility of the Department of Earth and Planetary Sciences (UNM) where Fleur Rietmeijer-Engelsman and Stacy Kaser provided technical support and W. Gong provided computer graphics expertise. NASA Grant NAG5-4441 supported this work.

REFERENCES CITED

Bradley, J.P. (1994) Chemically anomalous, pre-accretionally irradiated grains in interplanetary dust from comets. Science, 265, 925–929.

Bradley, J.P., Sandford, S.A., and Walker, R.M. (1988) Interplanetary dust particles. In J.F. Kerridge and M.S. Matthews, Eds., Meteorites and the Early Solar System, p. 861–895. University Arizona Press, Tucson.

Brownlee, D.E. (1985) Cosmic dust: Collection and research. Annual Review Earth Planetary Sciences, 13, 147–173.

Brownlee, D.E., Joswiak, D.J., and Bradley, J.P. (1999) High spatial resolution analyses of GEMS and other ultrafine grained IDP components (abstract). Lunar and Planetary Institute, Houston, (CD-ROM #2031).

Cliff, G. and Lorimer, G.W. (1975) The quantitative analysis of thin specimens. Journal Microscopy, 103, 203–207.

Dymek, R.F. and Gromet, L.P. (1984) Nature and origin of orthopyroxene megacrysts from the St-Urbain anorthosite massif, Quebec. Canadian Mineralogist, 22, 297–326.

Flynn, G.J. (1995) Thermal gradients in interplanetary dust particles: The effect of an endothermic phase transition (abstract). Lunar Planet Science, XXVI, 405–406.

Fockenberg, T. and Schreyer, W. (1997) Synthesis and chemistry of unusual excess-Si aluminous enstatite in the system MgO-Al_2O_3-SiO_2 (MAS). European Journal of Mineralogy, 9, 509–518.

Fraundorf, P. (1981) Interplanetary dust in the transmission electron microscope: diverse materials from the early solar system. Geochimica Cosmochimica Acta, 45, 915–943.

Fraundorf, P., Lyons, T., and Schubert, P. (1982) The survival of solar flare tracks in interplanetary dust silicates on deceleration in the earth's atmosphere. Proceedings of the 13th Lunar Planetary Science Conference, Journal of Geophysical Research, 87, Supplement, A409–A412.

Germani, M.S., Bradley, J.P., and Brownlee, D.E. (1990) Automated thin-film analyses of hydrated interplanetary dust particles in the analytical electron microscope. Earth and Planetary Science Letters, 101, 162–179.

Grossman, L. and Larimer, J.W. (1974) Early chemical history of the solar system. Reviews Geophysics Space Physics, 1, 71–101.

Huebner, J.S. (1980) Pyroxene phase equilibria at low pressure. In Mineralogical Society of America Reviews in Mineralogy, 7, 213–288.

Kerridge, J.F. and Matthews, M.S., Eds. (1988) Meteorites and the Early Solar System 1269 p. University Arizona Press, Tucson.

Love, S.G. and Brownlee, D.E. (1991) Heating and thermal transformation of micrometeoroids entering the Earth's atmosphere. Icarus, 89, 26–43.

Mackinnon, I.D.R. and Kaser, S.A. (1987) Microbeam analysis of clays at low temperature. In RH Geiss, Ed., Microbeam Analysis-1987, p. 332–334. San Francisco Press, California.

Mackinnon, I.D.R. and Rietmeijer, F.J.M. (1987) Mineralogy of chondritic interplanetary dust particles. Reviews Geophysics, 25, 1527–1553.

Mackinnon, I.D.R., McKay, D.S., Nace, G., and Isaacs, A.M. (1982) Classification of the Johnson Space Center Stratospheric Dust Collection. Proceedings of the 13th Lunar Planetary Science Conference, Journal of Geophysical Research, 87, Supplement, A413–A421.

Mysen, B.O., Virgo, D., and Kushiro, I. (1985) Experimental studies of condensation processes of silicate materials at low pressures and high temperatures, I. Phase equilibria in the system $CaMgSi_2O_6$-H_2 in the temperature range 1200–1500°C and the pressure range (P_{H_2}) 10^{-6} to 10^{-9} bar. Earth and Planetary Science Letters, 75, 139–146.

Nuth III, J.A, Hallenbeck, S.L., and Rietmeijer, F.J.M. (1999) Interstellar and Interplanetary Grains, Recent developments and new opportunities for experimental chemistry. In P. Ehrenfreund, K. Krafft, H. Kochan and V. Pirronello, Eds., Laboratory Astrophysics and Space Research, p. 143–182. Kluwer Academic Publisher, Dordrecht, the Netherlands.

Ramdohr, P. (1967) Die Schmelzkruste der Meteorieten. Earth and Planetary Science Letters, 2, 197–209.

Rietmeijer, F.J.M. (1987) Silicone oil: A persistent contaminant in chemical and spectral microanalyses of interplanetary dust particles (abstract). Lunar and Planetary Science Conference, XVIII, p. 836–837. Lunar and Planetary Institute, Houston.

———(1989) Ultrafine-grained mineralogy and matrix chemistry of olivine-rich chondritic interplanetary dust particles. Proceedings of the 19th Lunar and Planetary Science Conference, 513–521.

———(1996a) Cellular precipitates of iron-oxide in extraterrestrial olivine in a stratospheric interplanetary dust particle. Mineralogical Magazine, 60, 877–885.

———(1996b) The ultrafine mineralogy of a molten interplanetary dust particle as an example of the quench regime of atmospheric entry heating. Meteoritics and Planetary Science, 31, 237–242.

———(1998) Interplanetary dust particles. In Mineralogical Society of America Reviews in Mineralogy, 36, 2-1–2-95.

———(1999) Evolution of condensed pre-solar dust with metastable eutectic smectite dehydroxylate compositions: Truly GEMS (abstract). Lunar and Planetary Institute, Houston, (CD-ROM #1060).

Rietmeijer F.J.M. and Karner J.M. (1999) Metastable eutectics in the Al_2O_3-SiO_2 system explored by vapor phase condensation. Journal of Chemical Physics, 110, 4554–4558.

Rietmeijer, F.J.M. and Warren, J.L. (1994) Windows of opportunity in the NASA Johnson Space Center Cosmic Dust Collection. In M.E. Zolensky, T.L. Wilson, F.J.M. Rietmeijer and G.J. Flynn, Eds., Analysis of Interplanetary Dust, AIP Conference Proceedings, 310, p. 255–275. American Institute of Physics, New York, New York.

Rietmeijer, F.J.M., Karner, J.M., Nuth III, J.A. and Wasilewski, P.J. (1999a) Nanoscale phase equilibrium in a triggered lightning strike experiment. European Journal of Mineralogy, 11, 181–186.

Rietmeijer, F.J.M., Nuth III, J.A. and Karner, J.M. (1999b) Metastable eutectic gas to solid condensation in the FeO-Fe_2O_3-SiO_2 system. Physical Chemistry Chemical Physics, 1, 1511–1516.

Shinno, I. (1974) Unit cell dimensions and infra-red absorption spectra of Mg-wollastonite in the system $CaSiO_3$-$CaMgSi_2O_6$. Mineralogical Journal, 7(5), 456–471.

Stephens, J.R. and Kothari, B.K. (1978) Laboratory analogues to cosmic dust. Moon and Planets, 19, 139–152.

Warren, J.L. and Zolensky, M.E. (1994) Collection and curation of interplanetary dust particles recovered from the stratosphere. In M.E. Zolensky, T.L. Wilson, F.J.M. Rietmeijer, and G.J. Flynn, Eds., Analysis of Interplanetary Dust, AIP Conference Proceedings, 310, p. 105–114. American Institute of Physics, New York, New York.

Xu, H., Veblen, D.R., Luo, G., and Xue, J. (1996) Transmission electron microscopy study of the thermal decomposition of tremolite into clinopyroxene. American Mineralogist, 81, 1126–1132.

Zolensky, M. and Barrett, R. (1994) Compositional variations of olivines and pyroxenes in chondritic interplanetary dust particles. Meteoritics, 29, 616–620.

MANUSCRIPT RECEIVED JULY 13, 1998
MANUSCRIPT ACCEPTED JULY 13, 1999
PAPER HANDLED BY BRAD L. JOLLIFF